Numerical Simulation of a Brazed Plate Heat Exchanger using Al_2O_3-Water Nanofluid with Periodic Boundary Conditions

MADHU KALYAN REDDY PULAGAM, SACHINDRA KUMAR ROUT,
SUNIL KUMAR SARANGI
Department of Mechanical Engineering
C. V. Raman Global University,
Bidyanagar, Mahura, Bhubaneswar, Odisha-752054
INDIA

Abstract: - Brazed plate heat exchangers are used as evaporators, condensers, and single-phase heat exchangers in the industry. This complex piece of engineering has the effectiveness and compactness to give it an edge over many conventional heat exchangers. Solar power plants and organic Rankine cycle systems do use these heat exchangers as a part of heat recovery systems. The complex channels formed by the angled sinusoidal plates allow the fluid to be in a turbulent zone at a low Reynolds number, thus promoting better heat transfer characteristics. The challenge of simulating these heat exchangers is the large computational requirements. This can be solved by using periodic boundary conditions where a single repeating element is simulated to analyze the heat transfer characteristics of the entire channel. Varying concentrations of Al_2O_3 Nanofluid were considered as the working fluid for this study. The variation in the concentration did not affect the Nusselt number showing that the heat transfer coefficient was completely dependent on the hydraulic diameter and the thermal conductivity of the fluid. The friction factor also did not change with varying concentrations but the pressure drop increased as the chevron angle, pitch, and concentration increased.

Key-Words: - Brazed Plate, Heat Exchangers, Periodic boundary condition, CFD, friction factor, Nusselt number, HVAC.

Received: May 22, 2023. Revised: October 19, 2023. Accepted: December 11, 2023. Published: December 31, 2023.

1 Introduction

Brazed plate heat exchangers are made up of plates with sinusoidal corrugations stamped at an angle. These plates are stacked over one another in such a way that a channel forms in between the plates. The contact points of the two plates along with the edges are then brazed. This results in a complex zig-zag, rising and falling channels for the fluid to flow as shown in Figure 1. This promotes heat transfer to a much better degree than a flat plate heat exchanger. Many studies over the years have used different fluids for a variety of applications. Some studies included the use of refrigerants such as [1], and some have used water, [2]. While most of the studies were experimental, some CFD-based studies also gained prominence in analyzing the heat transfer characteristics of these heat exchangers. The present article focuses on the use of periodic boundary conditions, which allow the simulations to be performed at a faster rate and provide accurate results.

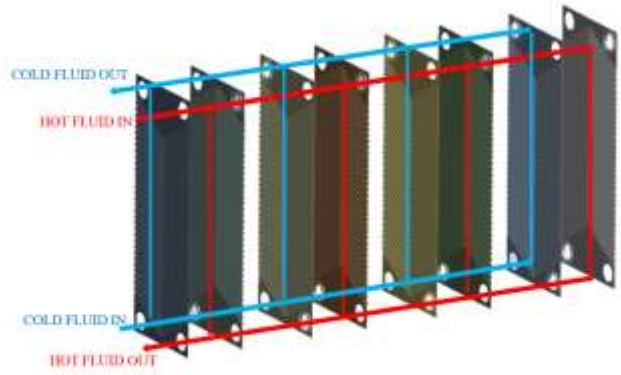

Fig. 1: Schematic of the plate arrangement and flow pattern

2 Literature Review and Objectives

CFD simulations to study the brazed plate heat exchangers alongside experimental work, [3]. The same heat exchanger was simulated with different turbulent models and determined that the turbulence model did not make a significant impact on the results, [4]. A plate heat exchanger with sinusoidal corrugations at low Reynolds numbers, [5],

simulated. The fluid was highly viscous and the resistances offered by the fluid increased with an increase in chevron angle. A plug flow was simulated in one dimension for a 4-channel plate heat exchanger, [6]. The k-ε turbulence model with enhanced wall treatment was used. Another work included simulation of small-sized PHE using the k-ε realizable model with non-equilibrium wall conditions, [7]. Milk as a working fluid was simulated to study the fouling and flow patterns of the plate heat exchangers used in the milk processing industry, [8] and [9] used the k-ω model and experimental analysis to observe the effect of chevron angles on the performance characteristics of BPHE.

Nanofluids were used in a couple of studies related to brazed plate heat exchangers. The heat transfer and pressure drop characteristics of one such nanofluid (TiO_2-water nanofluid) in a Brazed plate heat exchanger, [10] were investigated. Previous studies have published that the Nusselt number increased with the increase in the Reynolds number and volume fraction of the nanoparticles. characteristics of carbon-based nanofluids in BPHE under laminar flow, [11], was also studied. Two different concentrations were selected (0.2% wt. and 0.6% wt.) and their thermophysical properties such as thermal conductivity, and viscosity, were measured, analyzed and then the nanofluid was circulated inside a brazed plate heat exchanger to evaluate the average heat exchange capacity, pumping power consumption and system efficiency factor with inlet temperatures of 35, 40, and 45°C under laminar flow conditions. The system efficiency factor was slightly higher for lower concentration nanofluid than the higher one (7.98% as opposed to 7.28%) and considering all the properties and parameters the lower concentration nanofluid was recommended by the authors. the heat transfer and flow characteristics of a Multi-walled carbon nanotube - copper oxide (MWCNT-CuO) nanofluid in BPHE, [12], were studied and optimized. The nanofluid was compared with water as a cold fluid and was run through a test heat exchanger. An increase of 39.27% was calculated in the thermal conductivity. The friction factor increased slightly when compared with water. The same fluid, [13], was also studied for the thermal performance and flow analysis. A Nusselt number increase of 94% and a friction factor increase of 12.87% from the base fluid was reported. Energy consumption of H-type (larger chevron angle) and L-type (smaller chevron angle) brazed plate heat exchangers, [14], were compared and reported. The experiments were carried out at different flow rates of water. The H-type had better heat transfer as well as pressure drop at all flow rates but was more pronounced at higher flow rates.

3 Materials and Methods

Most of the CFD-based studies done have simplified the geometry in one way or another, [8], but some of them have simulated the entire geometry, [4]. These studies were done at the expense of high computational resources that an ordinary student might not have in possession. A close look at the geometry of the channel or the plates itself can reveal a pattern that repeats periodically. The end effects are not very significant since most of the heat transfer already happened in between the corrugations. Periodic boundary condition is an option in ANSYS Fluent which would simulate the effect of repeating patterns. This was taken as the key research methodology for this study. The repeated section length and width are modeled and simulated with constant heat flux conditions. A sinusoidal curve was created and extruded at an angle to create a plate. The same was done with an offset above the starting point of the original curve and rotated it to form the second plate. The region inside them was filled and the solid plates were deleted to retain the fluid medium. The remaining model was trimmed down to the periodic length and width. The geometry and periodic section are given in Figure 2. Simulations were designed for variation of pitch, amplitude-to-pitch ratio, chevron angle, and Reynolds number. Meshing was done in ICEM CFD since the default meshing module could create negative volume meshes. Using a block method in the ICEM CFD module it was easier to map out the mesh and then project it onto the curved surfaces to create a hexahedral structured mesh as shown in Figure 3. The grid independence test was done to identify the ideal number of elements and the sizing conditions used to create that mesh were considered for the remaining models. Laminar and standard k-ω SST models were used for the viscous models and the k-ω SST model was declared to be more suitable for computing a brazed plate heat exchanger, [4]. The convergence criteria were considered as 10^{-6} for all the residuals. A coupled discretization scheme was used with turbulence, energy, and pressure solvers at second-order discretization. The working fluid was taken as water with a constant heat flux condition given on the top and bottom walls. A sample model was simulated for grid independence and width independence test to check for the ideal mesh and dependence of width for the periodic conditions on the left and right walls. The results are

as given in Figure 4. The ideal mesh elements are around 3 x 10^6 elements since a 5% better result at higher angles is available at almost 2 - 2.5 times the selected size which increases the computation time drastically.

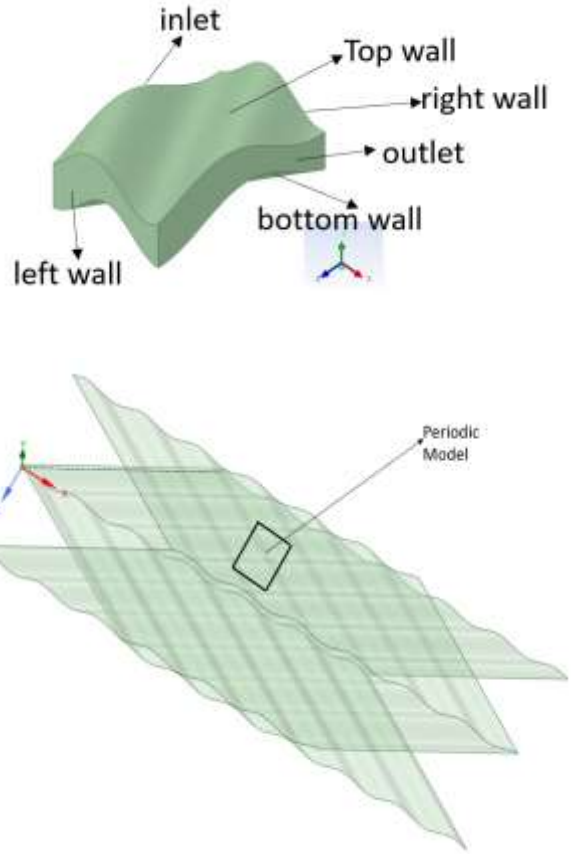

Fig. 2: Periodic model geometry

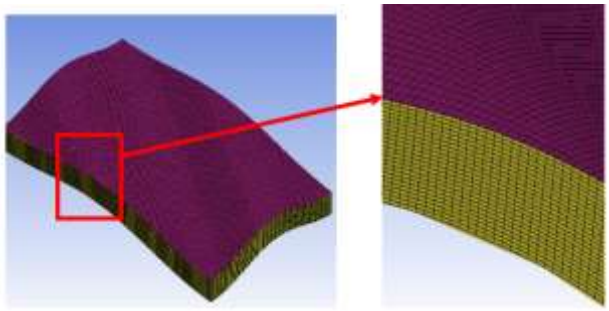

Fig. 3: Meshing of the model

The equations that were solved in the background are given in Eq. 1 – 11. The standard k-ω model is a two-equation model solved for turbulent flows, and the equations are given in Eq. 4 and 5. The SST version of this model accounts for the transport of the turbulence shear stress in the definition of turbulence viscosity as given in Eq. 6. The velocity in periodic flow is calculated as given in Eq. 7, 8, and 9, [15]. The pressure drop and temperature between the periodic faces are periodic and are calculated as given in Eq. 10 and 11, [15].

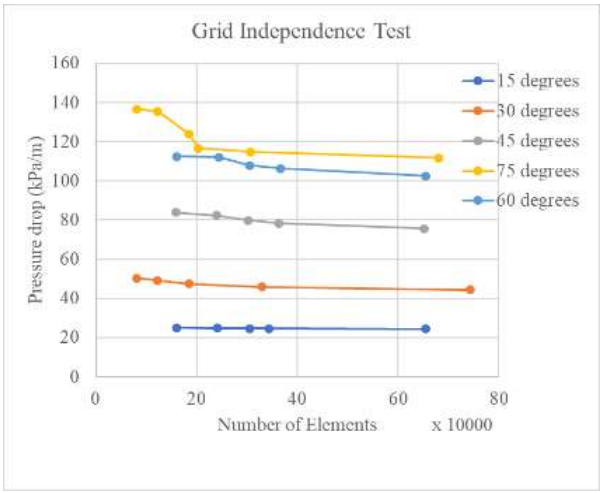

Fig. 4: Grid independence test

Continuity Equation

$$\frac{D\rho}{Dt} + \rho\nabla \cdot \vec{V} = 0 \tag{1}$$

Momentum Equation

$$\frac{\partial \rho u_i}{\partial t} + \frac{\partial}{\partial \lambda_j}\left(\rho u_j u_i - \tau_{ij}\right) = -\frac{\partial p}{\partial x_i} + s_i \tag{2}$$

Energy Equation

$$\rho\left[\frac{\partial h}{\partial t} + \nabla \cdot \left(h\vec{V}\right)\right] = -\frac{Dp}{Dt} + \nabla \cdot (k\nabla T) + \emptyset \tag{3}$$

$$\frac{\partial}{\partial t}(\rho k) + \frac{\partial}{\partial x_i}(\rho k u_i) = \frac{\partial}{\partial \lambda_j}\left(\Gamma_k \frac{\partial k}{\partial \lambda_j}\right) + G_k - Y_k + S_k \tag{4}$$

$$\frac{\partial}{\partial t}(\rho \omega) + \frac{\partial}{\partial x_i}(\rho \omega u_i) = \frac{\partial}{\partial \lambda_j}\left(\Gamma_\omega \frac{\partial \omega}{\partial \lambda_j}\right) + G_\omega - Y_\omega + S_\omega \tag{5}$$

$$\mu_t = \frac{\rho_k}{\omega}\frac{1}{max\left[\frac{1}{\alpha^*}, \frac{S_1 F_2}{\alpha_1 \omega}\right]} \tag{6}$$

$$F_2 = tanh[\phi_2^2]$$

$$\emptyset^2 = max\left[2\frac{\sqrt{k}}{0.09\omega y}, \frac{500\mu}{\rho y^2 w}\right]$$

$$u(\vec{r}) = u\left(\vec{r} + \vec{L}\right) = u\left(\vec{r} + 2\vec{L}\right) = \cdots \tag{7}$$

$$v(\vec{r}) = v\left(\vec{r} + \vec{L}\right) = v\left(\vec{r} + 2\vec{L}\right) = \cdots \tag{8}$$

$$w(\vec{r}) = w(\vec{r} + \vec{L}) = w(\vec{r} + 2\vec{L}) = \cdots \quad (9)$$

$$\Delta p = p(\vec{r}) - p(\vec{r} + \vec{L}) = p(\vec{r} + \vec{L}) - p(\vec{r} + 2\vec{L}) = \cdots \quad (10)$$

$$T(\vec{r}) = T(\vec{r} + \vec{L}) = T(\vec{r} + 2\vec{L}) = \cdots \quad (11)$$

$$\frac{\Delta p}{L} = \frac{4 f \rho v^2}{2 d_h} \quad (12)$$

$$Re = \frac{\rho v d_h}{\mu};\ d_h = \frac{4 \times V}{\text{As}};\ \dot{m} = \rho A_C v$$

$$Nu = \frac{h d_h}{k};\ h = \frac{Q}{A(T_s - T_b)} \quad (13)$$

The temperature and pressure drop data from Fluent are analyzed using Eq. 10 & 11 to get the friction factor and Nusselt numbers. Some sample cases were simulated to validate the results of the friction factor against the existing correlations, [14], as shown in Figure 5. The results fairly agreed with the calculated friction factor from the existing correlations except with low Re for Nu. The correlation underpredicted the value mainly due to the lack of consideration for the enlargement factor that results in a higher surface area for the plate heat exchanger.

The more accurate simulation of nanofluids should be using a multi-phase model. Due to the restrictions of the periodic boundary conditions without using a UDF, multi-phase flow is not possible. Thus, the properties of the nanofluid with Al_2O_3 particle size of 25 nm have been derived using a correlation from [16] and [17]. These properties are input as new fluids in ANSYS Fluent and then simulated to get more acceptable rather than accurate values. This is a small price to pay when looking at the huge computational requirements of simulating a 4 million-element full plate model. The fluid properties are given in Table 1.

.

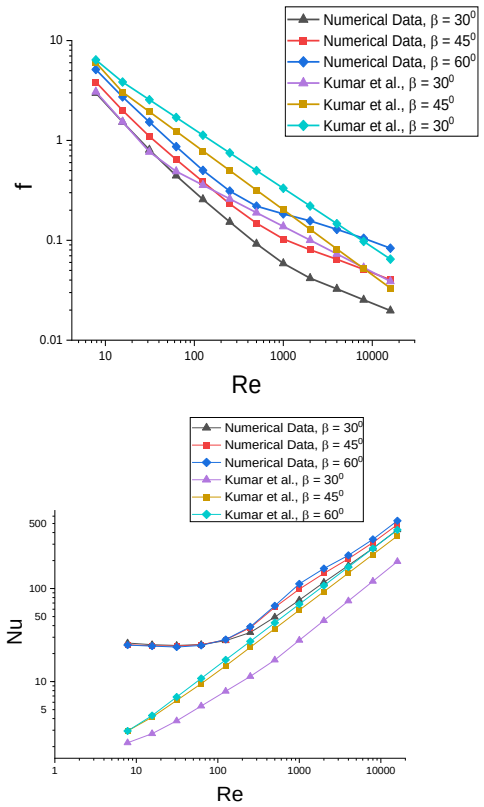

Fig. 5: Validation against experimental correlations given in [18]

Table 1. Al_2O_3 – water nanofluid properties

S. No	Volume fraction	Density (kg/m^3)	Dynamic viscosity (Pa-s)	Thermal conductivity (W/m-K)	Specific heat (J/kg-K)
1	0.5%	1009.17	0.000799	0.622	4119.51
2	0.75%	1015.93	0.000804	0.633	4089.87
3	1%	1022.69	0.000829	0.641	4060.62

4 Results and Discussion

The fluids are simulated through 5 different chevron angles (15° to 75°) of three different heat exchangers with pitches of 4 mm, 6 mm, and 8 mm and amplitude to pitch ratio of 0.2. the node data of each model is extracted and fed into a program that separates the values into each block of 100 equal blocks across the model. The bulk and surface temperature were averaged over each block and the entire block at the end to calculate the heat transfer coefficient and Nusselt number. The pressure drop values are a direct output of the periodic boundary

conditions, which are used to calculate the friction factor. As expected, the friction factor did not change its value with an increase in concentration. However, the value decreased with increasing Re and increased with increasing pitch and angle. Compared to plain water the friction factor was similar for the nanofluid and so was the pressure drop. The pressure drop was only slightly higher (less than 1% for the highest values) so the friction factor changes were also of a similar magnitude. Figure 6 shows the variation of friction factor and pressure drop for various chevron angles. It was also found that the friction factor increases 6 to 8 times from the lowest Re to the highest Re for the smallest angle of 115 degrees° and the highest angle of 75°. It was also observed that there was a maximum of 20% increase in friction factor as the pitch was increased and this was also mostly insignificant considering the absolute magnitude of the friction factor as shown in Figure 7.

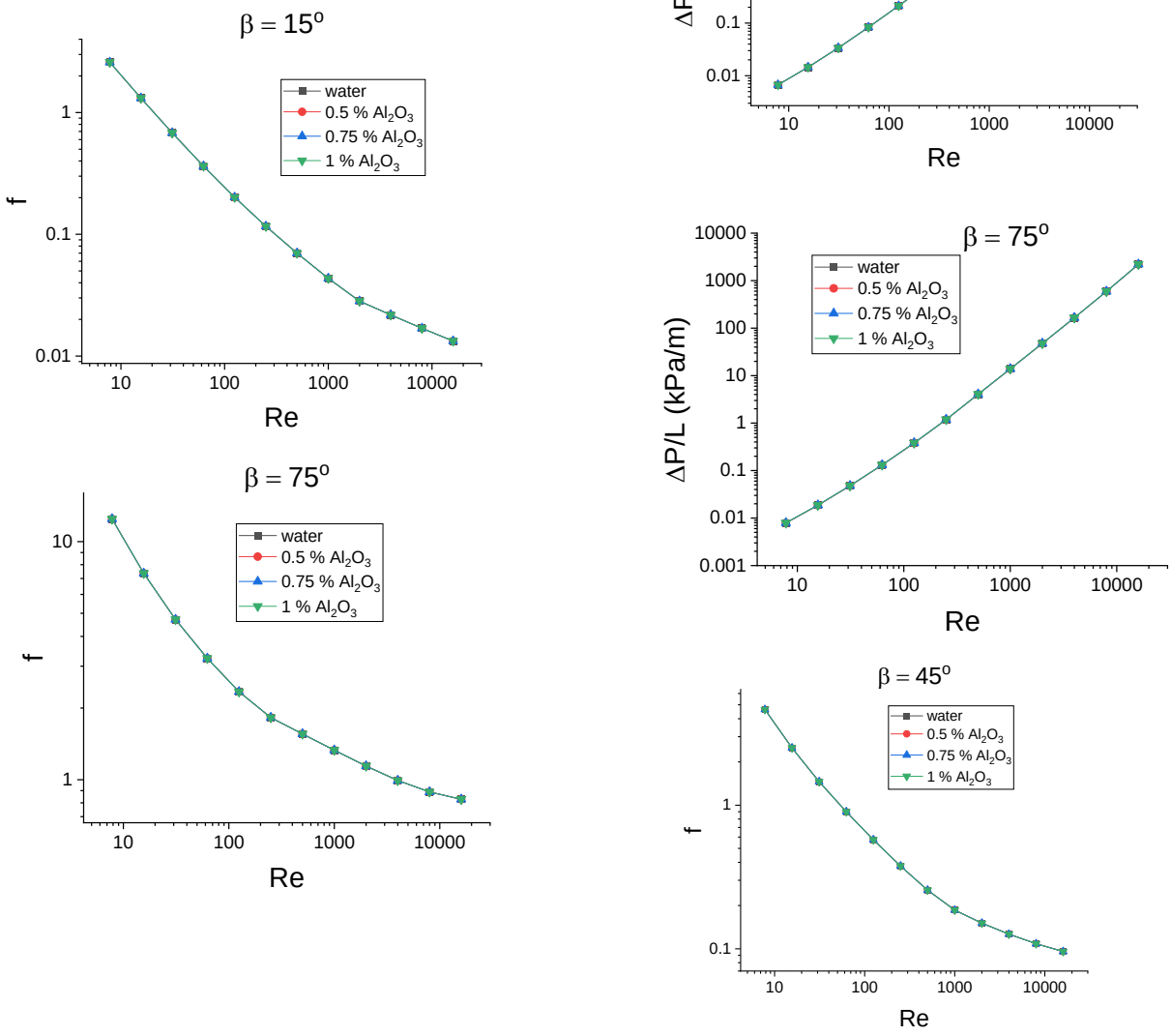

Fig. 6: f vs Re and Pressure drop per unit length vs Re for various β

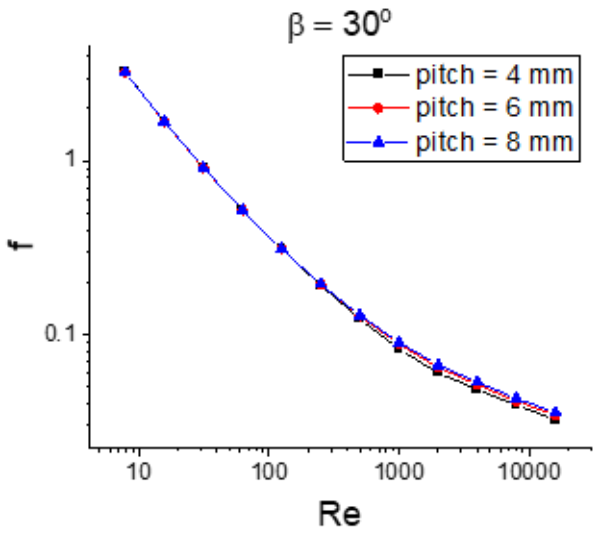

Fig. 7: f vs Re for various pitches of the corrugation

The effect of the different nanofluids was similar for the Nusselt number too. The values overlapped almost in all cases as shown in Figure 8. The increase in the Nu with Re was anywhere between 25 – 50 times depending on the chevron angle and the Reynolds number. At low Reynolds numbers, the Nusselt numbers were very similar to each other for all values of pitch and chevron angle. All the different concentrations have very similar Nu throughout with a maximum difference of 6%. Increasing the pitch had a similar effect on the Nusselt number where it was barely different for almost all Re as shown in Figure 9. [17], did give a different result to what was published in this article. The Nusselt number was the least for the distilled water and the maximum for the nanofluid with a 2% volume fraction. The major difference is the application where this nanofluid was used. It was used in a simulation of a shell and tube heat exchanger where the nanofluid was on the tube side with a uniform cross-section. The brazed plate heat exchanger is a completely different scenario. This shows that the Al_2O_3 nanofluid concentration under 1% does not make much of a difference in the pressure drop or the heat transfer coefficient. So, for economic reasons, it is better to use normal water.

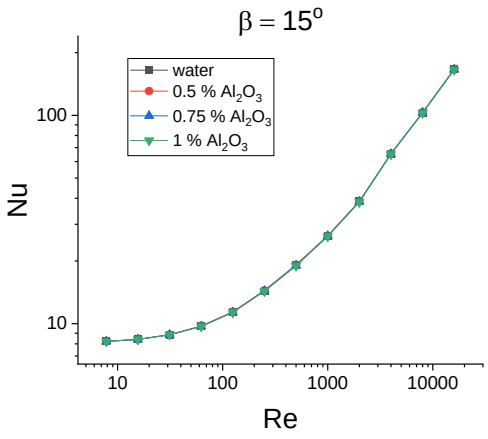

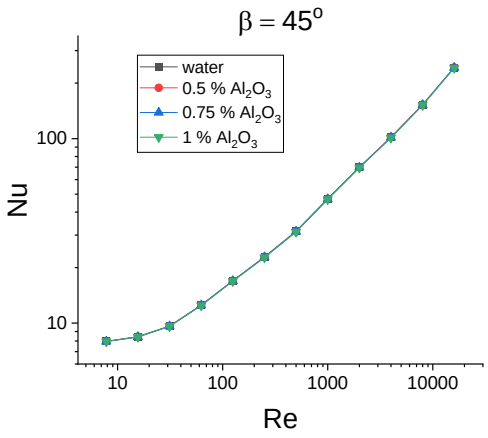

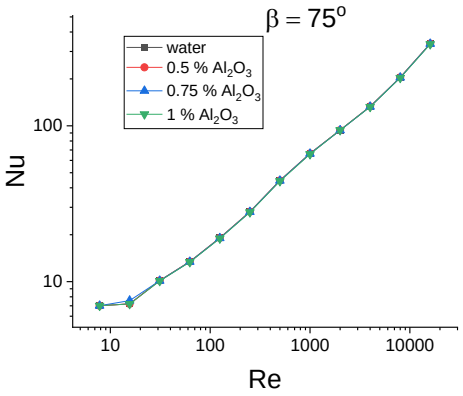

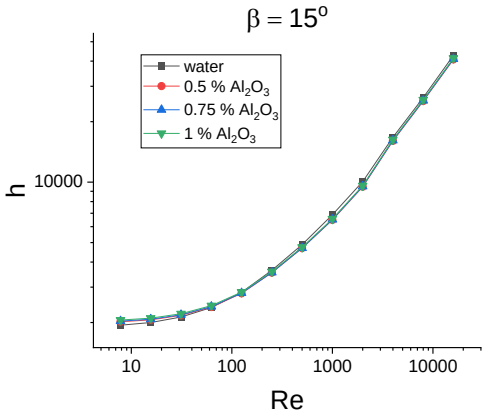

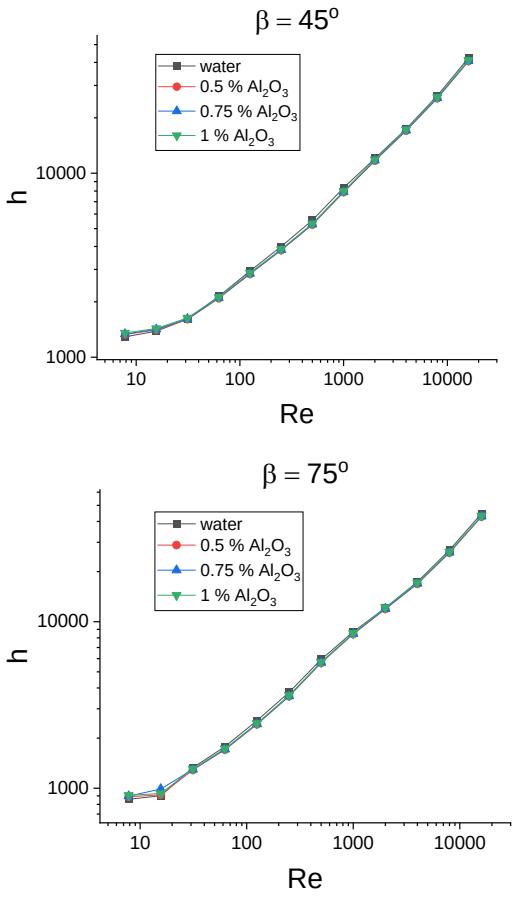

Fig. 8: Nu vs Re and heat transfer coefficient vs Re for various β

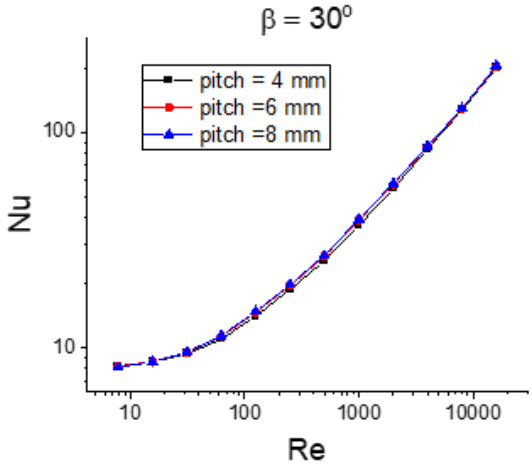

Fig. 9: Nu vs Re for various pitches of the corrugation

5 Conclusions

The Al_2O_3 nanofluid was used in the simulation of a braze plate heat exchanger for different chevron angles and pitches and the results were compared with water. The fluid properties were introduced into the fluent as a new homogeneous fluid and the simulations were carried out. Periodic boundary conditions were used to reduce the computational time and resources by decreasing the number of elements to 0.3 million when previous studies used models over 2 million elements.

- The friction factor increases 6 to 8 times from the lowest Re to the highest Re for the smallest angle of 15° and the highest angle of 75°. It was also observed that there was a maximum of 20% increase in friction factor as the pitch was increased.
- The Nusselt number slightly increased by about 2% from normal water for the nanofluid. All the different concentrations have very similar Nu throughout with a maximum increase of 6% from a lower to higher concentration.
- The brazed plate heat exchanger combined with nanofluids can work in areas requiring high heat load with small spaces such as Organic Rankine cycle systems. These systems generally require transfer at high heat loads in a limited space. Shell and tube or tube-in-tube heat exchangers cannot function as well as a brazed plate heat exchanger with its compactness and heat transfer properties.

Acknowledgement:
This work has been supported by the Board of Research in Nuclear Science (BRNS) under grant No. 59/14/03/2021-BRNS/57032. The authors are also grateful to Dr. Debakant Samal, Institute of Physics, Bhubaneswar, for our Principal collaborator for his continuous academic and technical support.

References:

[1] G. A. Longo, "Heat transfer and pressure drop during hydrocarbon refrigerant condensation inside a brazed plate heat exchanger," *Int. J. Refrig.*, vol. 33, no. 5, pp. 944–953, 2010, doi: 10.1016/j.ijrefrig.2010.02.007.

[2] W. Han, K. Saleh, V. Aute, G. Ding, Y. Hwang, and R. Radermacher, "Numerical simulation and optimization of single-phase turbulent flow in chevron-type plate heat exchanger with sinusoidal corrugations," *HVAC R Res.*, vol. 17, no. 2, pp. 186–197, 2011, doi: 10.1080/10789669.2011.558167.

[3] V. Sekhar Gullapalli, "Doctoral Thesis. Estimation of Thermal and Hydraulic Characteristics of Compact Brazed Plate Heat Exchangers. Lund University, Sweden.," *PhD Lund*, 2013, [Online]. Available: http://lup.lub.lu.se/record/3799250/file/3799358.pdf (Accessed Date: January 2023).

[4] V. S. Gullapalli and B. Sundén, "Cfd simulation of heat transfer and pressure drop in compact brazed plate heat exchangers," *Heat Transf. Eng.*, vol. 35, no. 4, pp. 358–366, 2014, doi: 10.1080/01457632.2013.828557.

[5] J. Fernández-Seara, R. Diz, and F. J. Uhía, "Pressure drop and heat transfer characteristics of a titanium brazed plate-fin heat exchanger with offset strip fins," *Appl. Therm. Eng.*, vol. 51, no. 1–2, pp. 502–511, 2013, doi: 10.1016/j.applthermaleng.2012.08.066.

[6] F. C. C. Galeazzo, R. Y. Miura, J. A. W. Gut, and C. C. Tadini, "Experimental and numerical heat transfer in a plate heat exchanger," *Chem. Eng. Sci.*, vol. 61, no. 21, pp. 7133–7138, 2006, doi: 10.1016/j.ces.2006.07.029.

[7] S. Jain, A. Joshi, and P. K. Bansal, "A new approach to numerical simulation of small sized plate heat exchangers with chevron plates," *J. Heat Transfer*, vol. 129, no. 3, pp. 291–297, 2007, doi: 10.1115/1.2430722.

[8] K. Grijspeerdt, B. Hazarika, and D. Vucinic, "Application of computational fluid dynamics to model the hydrodynamics of plate heat exchangers for milk processing," *J. Food Eng.*, vol. 57, no. 3, pp. 237–242, 2003, doi: 10.1016/S0260-8774(02)00303-5.

[9] S. Muthuraman, "The Characteristics of Brazed Plate Heat," *Glob. J. Res. Eng. Mech. Mech. Eng.*, vol. 11, no. 7, pp. 11–26, 2011.

[10] R. Barzegarian, M. K. Moraveji, and A. Aloueyan, "Experimental investigation on heat transfer characteristics and pressure drop of BPHE (brazed plate heat exchanger) using TiO2-water nanofluid," *Exp. Therm. Fluid Sci.*, vol. 74, pp. 11–18, 2016, doi: 10.1016/j.expthermflusci.2015.11.018.

[11] T. P. Teng, T. C. Hsiao, and C. C. Chung, "Characteristics of carbon-based nanofluids and their application in a brazed plate heat exchanger under laminar flow," *Appl. Therm. Eng.*, vol. 146, pp. 160–168, 2019, doi: 10.1016/j.applthermaleng.2018.09.125.

[12] I. Fazeli, M. R. Sarmasti Emami, and A. Rashidi, "Investigation and optimization of the behavior of heat transfer and flow of MWCNT-CuO hybrid nanofluid in a brazed plate heat exchanger using response surface methodology," *Int. Commun. Heat Mass Transf.*, vol. 122, p. 105175, 2021, doi: 10.1016/j.icheatmasstransfer.2021.105175.

[13] H. Mehrarad, M. R. Sarmasti Emami, and K. Afsari, "Thermal performance and flow analysis in a brazed plate heat exchanger using MWCNT@water/EG nanofluid," *Int.Commun. Heat Mass Transf.*, vol. 146, no. December 2022, p. 106867, 2023, doi: 10.1016/j.icheatmasstransfer.2023.106867.

[14] S. Gungor, "Experimental comparison on energy consumption and heat transfer performance of corrugated H-type and L-type brazed plate heat exchangers," *Int. Commun. Heat Mass Transf.*, vol. 144, p. 106763, 2023, doi: 10.1016/j.icheatmasstransfer.2023.106763.

[15] ANSYS Inc, ANSYS Fluent Theory Guide 12.0, 2015, [Online]. https://www.afs.enea.it/project/neptunius/docs/fluent/html/th/main_pre.htm (Accessed Date: February 26, 2024).

[16] B. C. Pak and Y. I. Cho, "Hydrodynamic and heat transfer study of dispersed fluids with submicron metallic oxide particles," *Exp. Heat Transf.*, vol. 11, no. 2, pp. 151–170, 1998, doi: 10.1080/08916159808946559.

[17] K. Somasekhar, K. N. D. Malleswara Rao, V. Sankararao, R. Mohammed, M. Veerendra, and T. Venkateswararao, "A CFD Investigation of Heat Transfer Enhancement of Shell and Tube Heat Exchanger Using Al_2O_3-Water Nanofluid," *Mater. Today Proc.*, vol. 5, no. 1, pp. 1057–1062, 2018, doi: 10.1016/j.matpr.2017.11.182.

[18] H. Kumar, Plate Heat Exchanger: Construction and Design, no. 86. The Institution of Chemical Engineers, 1984. doi: 10.1016/b978-0-85295-175-0.50054-0.

NOMENCLATURE

A_C	Cross-sectional area	[m^2]
A_s	Surface area	[m^2]
d_h	Hydraulic diameter	[mm]
h	Heat transfer Coefficient	[W/m^2-K]
f	Friction factor	--
k	Turbulence kinetic energy	[J]
K	Thermal conductivity	[W/m-K]
L	Length	[m]
$\vec{L}$	Periodic length	[m]
$\dot{m}$	Mass flow rate	[kg/s]
Nu	Nusselt Number	--
p	Pressure	[Pa]
P	Pitch	[m]
Δp	Pressure gradient	[Pa/m]
Q	Heat flux	[W/m^2]
$\vec{r}$	Position vector	--
Re	Reynolds number	--
S	Source term	--
S_1	Strain magnitude	--
t	Time	[s]
T	Temperature	[K]
T_b	Bulk Temperature	[K]
T_s	Surface Temperature	[K]
$u(\vec{r})$	Velocity field in x direction	[m/s]
$v(\vec{r})$	Velocity field in y direction	[m/s]
$\vec{V}$	Velocity field	[m/s]
$w(\vec{r})$	Velocity field in z-direction	[m/s]
v	Average velocity	[m/s]
Y	Dissipation term due to turbulence	--
y	Distance to the next surface	[m/s]
ρ	Density	[kg/m^3]
ϕ	Area enlargement factor	--
Γ	Effective diffusivity	[m^2/s]
ω	Specific dissipation rate	[m^2/s^3]
α^*	Coefficient of damp turbulent viscosity	--
ϕ	Fin height (H) to width (s) ratio	--
μ	Viscosity	[Pa-s]

Contribution of Individual Authors to the Creation of a Scientific Article (Ghostwriting Policy)

- Madhu Kalyan Reddy Pulagam,: simulation and experimental test rig set up,
- Sachindra Kumar Rout: Manuscript preparation and result analysis
- Sunil Kumar Sarangi: Idea generation and draft correction

Sources of Funding for Research Presented in a Scientific Article or Scientific Article Itself

This work has been supported by the Board of Research in Nuclear Science (BRNS) under grant No. 59/14/03/2021-BRNS/57032. The authors are also grateful to Dr. Debakant Samal, Institute of Physics, Bhubaneswar, for our Principal collaborator for his continuous academic and technical support.

Conflict of Interest

The authors have no conflicts of interest to declare.